

Research

**Cite this article:** Commins T, Siviour CR. 2023Stress relaxation after low- and high-rate deformation of polyurethanes. *Proc. R. Soc. A***479:** 20220830.<https://doi.org/10.1098/rspa.2022.0830>

Received: 13 December 2022

Accepted: 20 June 2023

Subject Areas:

materials science, mechanical engineering

Keywords:

polyurethane, relaxation, high strain rate

Author for correspondence:

Tom Commins

e-mail: thomas.commins@magd.ox.ac.ukElectronic supplementary material is available online at <https://doi.org/10.6084/m9.figshare.c.6729720>.

Stress relaxation after low- and high-rate deformation of polyurethanes

Tom Commins and Clive R. Siviour

Department of Engineering Science, University of Oxford, Parks Road, Oxford OX1 3PJ, UK

TC, 0000-0002-9407-4654

Polymers possess a wide range of mechanical behaviours depending upon the temperature and loading rate. An often-overlooked aspect is relaxation, important because it acts over a wide range of time periods and begins as soon as the polymer is loaded. In the research presented, the relaxation behaviour of two polyurethanes (PUs) following deformation was investigated at low-rate, 10^{-3} s^{-1} , and dynamic, 10^3 s^{-1} , loading rates, with the former exploring temperatures from 20°C to -60°C . These are compared to a predictive Prony series model calibrated using mastercurves produced by applying time-temperature superposition to data obtained using a dynamic mechanical analysis machine. For relaxation after dynamic loading, a recently proposed analysis was used to account for the movement of the bars during relaxation. The model could predict the stress-time response after low-rate deformation to strains of 2%, at all temperatures. As the strains increased, irrecoverable deformation was observed and the model became less accurate. In the dynamic experiments, the model accurately predicted the early stages of relaxation for both PUs but deviated later on. A modification was suggested to account for these observations. Further characterization of the mechanical response under large strain compressive loading is also reported.

1. Introduction

Polymers are used in many applications that experience mechanical deformation over an extensive range of loading rates and temperatures, from quasi-static to

ballistic impact [1–6]. The properties of most polymers vary significantly with loading rate and temperature, with variations of three orders of magnitude in stiffness not uncommon [7,8]. Understanding the temperature and rate dependence of the polymer across relevant conditions is therefore essential. An often-overlooked aspect of polymer behaviour is the relaxation, which acts over all time periods and begins as soon as the polymer is loaded. Therefore, it is particularly important to understand this behaviour, especially because it is inherently energy-dissipative and could be influential in energy-absorptive applications.

In general, stress relaxation in polymers occurs through chemical and mechanical mechanisms, including chain scission, bond interchange, molecular entanglement, viscous flow and motion by reptation [9–13]. For the mechanical motion of polymer chains, there is an associated internal friction as the chains slide past each other. This drag force rises to a peak during the polymer's glass transition before decreasing. Additional smaller peaks in drag are observed at the secondary transitions [14]. Depending on the loading and environmental conditions, any combination of these mechanisms could be significant during relaxation. Phenomenologically, relaxation can be described in a model using a combination of elastic springs and viscous dashpots. In this research, a Prony series, an extension of the generalized Maxwell model [15–17] consisting of parallel branches of spring-dashpot pairs, is used.

To calibrate the model, dynamic mechanical analysis (DMA) is used. This experimental procedure measures the frequency and temperature dependence of the complex modulus and the ratio of stored energy to dissipated internal energy (i.e. the loss tangent) in the polymer. For a comprehensive review, see [18]. The principle of time-temperature superposition can be applied to these results to create a mastercurve of stiffness at a single-reference temperature [19] to which the Prony material model can be fitted. A limitation is that the DMA investigates only the small-strain behaviour, and time-temperature superposition can only be used for this purpose in the linear-viscoelastic regime; therefore, other methods of measuring the large strain response are required.

To determine the large strain, high-strain rate properties of polymers, a Split Hopkinson Pressure Bar (SHPB) can be used [20–24]. In conventional SHPB, a stress pulse is created from the impact of a striker on an input bar. This 'incident pulse' interacts with the specimen producing reflected and transmitted pulses that can be used to determine the stress-strain properties of the material. Of interest to this project is the period post-loading during which the specimen can relax [25].

The work reported in the current paper aims to determine the ability of the Prony series model, fitted using DMA data, to predict the relaxation behaviour of two polymers at microsecond and hundreds of second timescales. In order to achieve this, two representative polyurethane (PU) materials were obtained with different glass transition temperatures, one above (50°C) and one below (15°C) room temperature. The specimens were first characterized using DMA and large strain compression experiments at different strain rates and temperatures. Then, relaxation experiments were performed following low-rate and dynamic deformation. This allowed the performance of this model to be explored with variations in the temperature, strain rate and final strain, while at the same time considering both rubbery and glassy behaviours.

2. Materials

Two PUs, commercially known as 'Task 3' and 'Task 11', were sourced from Bentley Advanced Materials [26]. The polymers were selected to have different glass transition temperatures while maintaining chemical similarity. Task 3 has a glass transition temperature of 55°C; Task 11, 15°C measured using differential scanning calorimetry (DSC) where the materials were heated from -90°C to 120°C at $3^{\circ}\text{C min}^{-1}$, see electronic supplementary material, Appendix. The PUs were obtained as two-part polymers and, once mixed and degassed, were cured in moulds to produce rectangular plates. The polymers were allowed to cure at room temperature for 24 h before a final post-cure heat treatment at 65°C for 4 h per the manufacturer's instructions. Once cured, the

polymer sheets were fly-cut flat to approximately 3.5 mm thickness, and circular specimens of either 6 or 10 mm diameter were cut from the sheets using a CNC mill.

In this study, 2–3 specimens of each polymer were investigated across each of 19 distinct loading and environmental conditions.

3. Experimental procedure

Three sets of experiments were performed:

Dynamic mechanical analysis—conducted as part of the thermomechanical analysis. A Prony series was fitted to these data.

Compression—specimens were compressed at low- and high-strain rates. The low-rate experiments were conducted at ambient and sub-ambient temperatures. These were to characterize the polymer's response to rate and temperature.

Relaxation—specimens were loaded to pre-determined strains or loads at low and high rates and allowed to relax. The low-rate relaxation experiments were conducted at ambient and sub-ambient conditions. These results were compared against Prony model predictions.

(a) Dynamic mechanical analysis

DMA was used to investigate the polymers' thermomechanical properties at low strains. Two configurations were used: single cantilever in oscillation different frequencies and temperatures, and three-point bend under isothermal relaxation.

For the single-cantilever frequency sweeps, prismatic specimens of dimensions approximately $17.5 \times 12.1 \times 3.45$ mm were oscillated with a 0.1% strain amplitude at 0.1 Hz, 0.32 Hz, 1 Hz, 3.16 Hz and 10 Hz. This was performed isothermally at temperatures from -70°C to $+70^\circ\text{C}$ in 2.5°C intervals. Specimens were held at each temperature interval for 5 min before loading to ensure isothermal conditions.

For the relaxation experiments, prismatic specimens of approximately $55 \times 12.1 \times 3.3$ mm were loaded in a three-point bend configuration. A stress relaxation testing procedure was used. Here, specimens were loaded slowly in three-point bend to 0.1% strain. They were then held for 10 min, during which time the required force was recorded. The polymer was then allowed to recover, unloaded, for 20 min before repeating the experiment at a new temperature. Measurements were made from -85°C to $+55^\circ\text{C}$ in 5°C intervals.

From these data, time-temperature superposition was used to create a mastercurve, which describes the storage modulus of the polymer over a far greater time range than can be tested experimentally. This mastercurve was used to calibrate a Prony series using the procedure described in §5.1.

(b) Compression

(i) Low-rate compression

The low-rate response of the polymers was investigated using a commercial screw-driven testing machine (Instron 3400 Series), instrumented with a contacting extensometer attached to the loading platens close to the specimen. To reduce friction between the specimen and platen faces, AEROSPEC 201 Graphited grease was used. This screw-driven apparatus was used to compress cylindrical specimens of 10 mm diameter and 3.5 mm height to 50% true strain. Experiments were performed over a range of strain rates at room temperature and at a range of temperatures at 10^{-2} s^{-1} , table 1.

Table 1. Experimental conditions for low-rate compression.

	strain rate	final true strain	temperature
varying strain rate	$10^{-1}, 10^{-2}, 10^{-3}$	0.5	20°C
varying temperature	10^{-3}	0.5	−60°C, −40°C, −20°C, 0°C, 20°C

Table 2. Low-rate stress relaxation experimental conditions for Task 11.

	varying temperature				varying final strain		
temperature (°C)	−60	−40	−20	0	20	20	20
loading stress (MPa)	53	53	33	20	2.7	—	—
loading strain (%)	—	—	—	—	(6)	10	15

(ii) High-rate compression

To characterize the polymer response under high-rate loading, a Split Hopkinson Pressure Bar was used following the methodology proposed by Cloete [25]. In this project, the bars were made from a Titanium alloy (Ti6Al4V) and were 12.7 mm in diameter. The striker bar was 400 mm long, the input bar 1000 mm and the output bar 500 mm long. Strain gauges were bonded to the input and output bars to measure the incident, transmitted and reflected waves. These data were then used to calculate the strain and stress in the specimen using the standard equations, see [21] for a full analysis. The specimens were 6 mm in diameter and 3.5 mm thick. Vaseline was used to lubricate the contact between the polymer and bar faces.

(c) Relaxation

(i) Low-rate relaxation

Further experiments were conducted to investigate the stress relaxation of the polymer over 100 s following low-strain rate deformation. The specimens (3.5 mm height and 10 mm diameter) were first compressed in the screw-driven testing machine to a pre-determined force at a strain rate of 10^{-3} s^{-1} . Then, the crosshead was held in place for 600 s. The force supported by the specimen was recorded, allowing the specimen’s relaxation behaviour to be measured under fixed boundary conditions. The force was chosen to be within the linear-viscoelastic regime for each polymer and corresponded to 2% strain, so it was therefore temperature-dependent. The experiment was performed from 20°C to −60°C in 20°C intervals.

A further investigation was conducted into the relaxation behaviour at larger strains: 10% and 15% for Task 11; 4% and 10% for Task 3. Here, the specimen was loaded until the desired strain, chosen to match the final strains observed in the high-rate stress relaxation experiments. At the larger strains, nonlinear effects such as plasticity were observed; therefore, a final load condition could not be used. For these experiments, a pre-load of 50 N was applied to the specimens before the experiment was conducted to remove end effects and ‘bedding in’ at the start of the experiment, allowing the specimens to be reliably loaded to a known strain.

This experimental procedure is summarized in tables 2 and 3.

(ii) High-rate relaxation

To investigate the microsecond timescale relaxation behaviour of the polymers, further SHPB experiments were performed. The experimental configuration was the same as described above; however, the striker bar was shortened to 250 mm to give a shorter loading duration. Thus, after the input pulse interacted with the specimen, there was a period of time in which the specimen could relax. This relaxation exerted a force on the confining input and output bars, measured

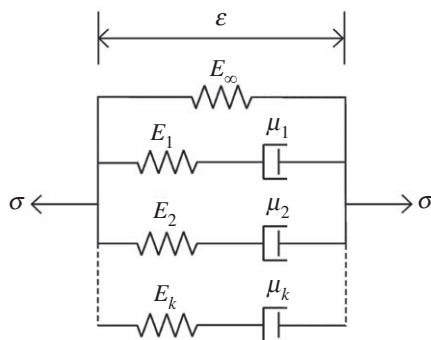


Figure 1. Spring-dashpot representation of a k -branch Prony series.

Table 3. Low-rate stress relaxation experimental conditions for Task 3.

	varying temperature				varying final strain		
temperature (°C)	−60	−40	−20	0	20	20	20
loading stress (MPa)	66	66	53	53	33	—	—
loading strain (%)	—	—	—	—	(2)	4	10

using the strain gauges. Experiments were performed at 20°C on specimens 3.5 mm in height and either 10 mm or 6 mm in diameter. Two specimen sizes were chosen to allow an investigation into the influence of the final loading strain on the subsequent relaxation behaviour to be conducted.

4. Modelling

(a) Prony series representation

Polymers are viscoelastic materials; hence, they exhibit different behaviour depending upon the timescale over which the load is applied. Therefore, a material model that captures this time-dependent behaviour is required and, for this project, a Prony series, which is a well-established model, was used. Represented schematically in figure 1, a general k -branched Prony series consists of a number of branches in parallel, with each branch containing a spring-dashpot pair in series, where the springs have stiffness, E , and the dashpots have viscosity, μ . The branches represent different relaxations in the polymer.

The constitutive model for this Prony series representation can be derived initially through a force balance along each branch. A Laplace transform can then be taken, and the initial conditions applied. See [15,27] for detailed descriptions. Under a step strain input, ϵ_0 , the stress relaxation behaviour can be represented by

$$\frac{\sigma(t)}{\epsilon_0} = E(t) = E_\infty + \sum_{n=1}^k E_n e^{-(t/\tau_n)}, \quad (4.1)$$

where

$$\tau_n = \frac{\mu_n}{E_n}, \quad (4.2)$$

where σ and ϵ are the stress and strain in the material, t is the time and τ is the characteristic time constant for each branch. For more general loading cases, the complexity increases because

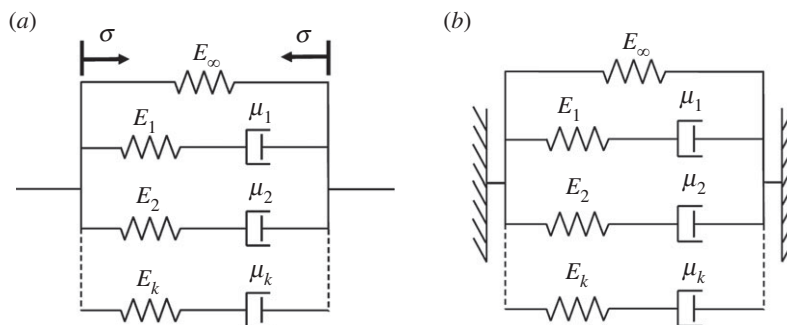


Figure 2. Boundary condition of the Prony model representation under low-rate loading and relaxation. During loading, stress-time boundary conditions measured experimentally were applied to the model. (a) Loading and (b) Relaxation.

relaxation of the model will begin as soon as the loading starts. Therefore, for a general case

$$\sigma(t) = \varepsilon(0+)E(t) + \int_0^t E(t-s)\dot{\varepsilon}(s) ds, \quad (4.3)$$

where s is a dummy variable representing time. A single-element model was created in ABAQUS to solve this equation during loading and relaxation. The model was used as a tool to solve the constitutive equations of a Prony series and not as a separate comparison to the experiment. In order to achieve this, the single-element ABAQUS model was given material properties corresponding to the calibrated Prony series and relevant boundary conditions, described below, corresponding to the experiments performed, were applied, allowing the stress response to be calculated. To ensure the ABAQUS model was in one-dimensional stress, no lateral confinement was applied, and the density of the material model was selected to be artificially small to remove any parasitic effects of inertia under dynamic loading. This method was verified by initially considering an arbitrary two-branch Prony model whose solution can be determined by hand.

(b) Low-rate stress relaxation modelling

The model boundary conditions were applied as follows (see also figure 2). The model was deformed using the experimentally observed stress-time relationship until it achieved the peak stress measured in the experiments. Then, the boundaries were fixed and the polymer was allowed to relax. The force at the boundaries was output from the model. The advantage of this method was that, experimentally, it is easier to measure the forces accurately than the specimen displacements, owing to compliance in the load frame and end effects on the specimen (e.g. non-parallel specimen faces, effects of the lubricant layer). At large deformations, if plasticity was observed in the experiment, it was assumed that the plastic deformation did not contribute to the subsequent relaxation—only the viscoelastic deformation relaxed. Hence, no plasticity model was required.

(c) High-rate relaxation modelling

For loading, the experimentally observed stress-time profile was again used as the models' boundary condition. Under relaxation, the analysis of Cloete *et al.* was used [25]. Here, the confining presence of the input and output bars can restrict, but not prevent, the expansion of the specimen during its relaxation. Because the bar movement is governed by wave propagation, the stress is proportional to the velocity. Hence, during relaxation, the specimen can be modelled as though the boundaries of this material are attached to two confining dashpots. The boundary

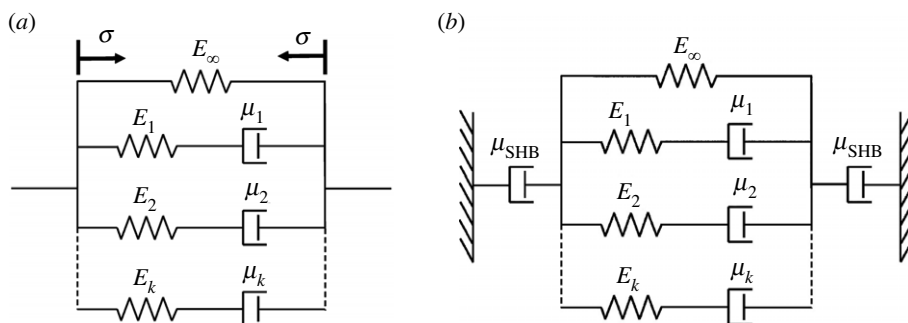


Figure 3. Boundary condition of a Prony model representation under high-rate loading and relaxation. During loading, stress-time boundary conditions measured experimentally were applied to the model. During relaxation, the boundaries of the Prony model move as though limited by the action of two dashpots [24]. (a) Loading and (b) Relaxation.

conditions under loading and unloading are represented schematically in figure 3*a,b*. The dashpots have been shown to have a viscosity of

$$\mu_{SHB} = \frac{1}{2} L_s \frac{A_b}{A_s} \rho_b c_b, \quad (4.4)$$

where L_s is the length of the specimen, A_b and A_s are the area of the bar and specimen, respectively, and ρ_b and c_b are the bar's density and elastic wave speed, respectively [25]. The analysis used to derive equation (4.4) was conducted using a symmetrical half model; therefore, in this study, in which the full specimen geometry is considered, two dashpots have been used, figure 3*b*.

5. Results and discussion

(a) Dynamic mechanical analysis

DMA was performed in two configurations: frequency sweeps on single-cantilever specimens and stress relaxation on three-point bend specimens. Mastercurves were produced using both sets of data. The full procedure is shown here for the stress relaxation data; however, an identical procedure was followed for single-cantilever DMA, the results from which can be found in the electronic supplementary material, Appendix.

The raw relaxation data for both polymers are displayed in figure 4, where each line represents data obtained at a temperature between -85°C and $+55^{\circ}\text{C}$, in 5°C increments. At each temperature, the evolution of the relaxation modulus with time was measured and the temperatures of interest around the glass transition temperature have been marked. Away from these temperatures, where there was considerably less temperature dependency, significant grouping of the data was found. The principal of time-temperature superposition was then implemented to produce a stiffness mastercurve [19]. To generate this mastercurve, all the curves for each temperature were horizontally shifted on the time axis to overlap with the data taken at a reference temperature, chosen here to be 20°C . The magnitude of this shift was dependent upon the temperature and these shift factors required are presented in figure 5. Once all the data were overlain, this produced the mastercurve in figure 6. On this figure, both mastercurves from the single-cantilever and three-point bend configurations are presented.

It is evident that there are significant differences in the mastercurves in figure 6: the DMA configuration strongly influences the overall results. Broadly, it was observed that the single-cantilever DMA produces a lower modulus than the three-point bend. Deng *et al.* [28] observed the same effect and found that the three-point bend DMA modulus agreed better with moduli obtained from tensile experiments at various temperatures. This could be attributed to differences

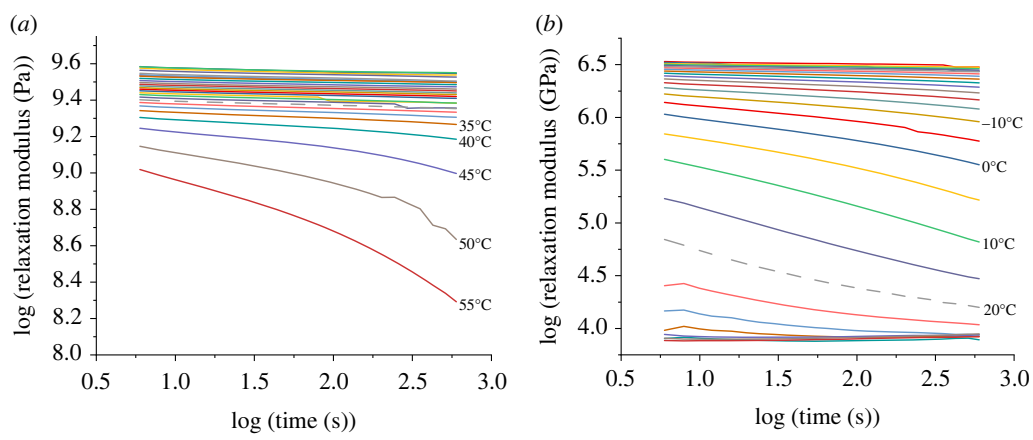


Figure 4. Relaxation DMA data. The reference temperature 20°C has been presented by a dashed line. (a) Task 3 and (b) Task 11.

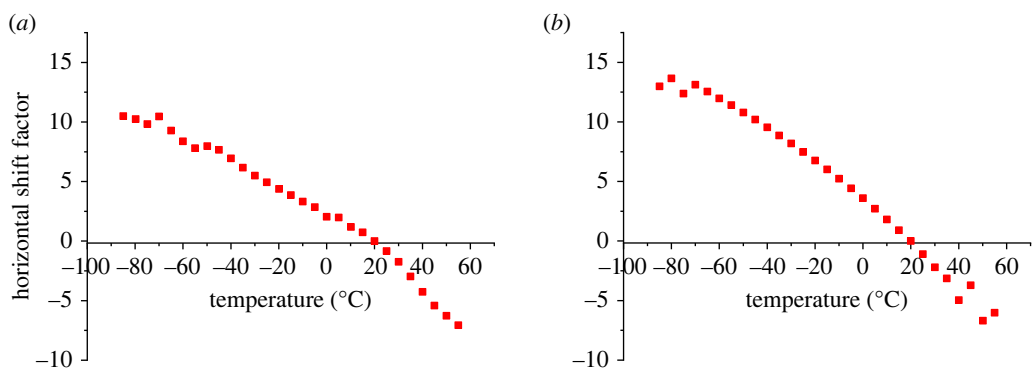


Figure 5. Shift factors used to produce relaxation mastercurve at 20°C. (a) Task 3 and (b) Task 11.

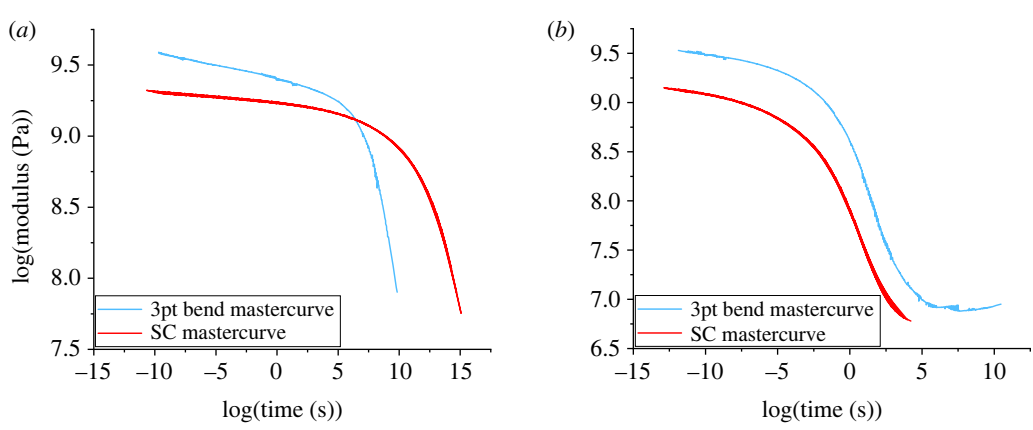


Figure 6. Comparison of 20°C mastercurves produced using relaxation data in the three-point bend configuration or oscillatory in single-cantilever (SC) configuration. (a) Task 3 and (b) Task 11.

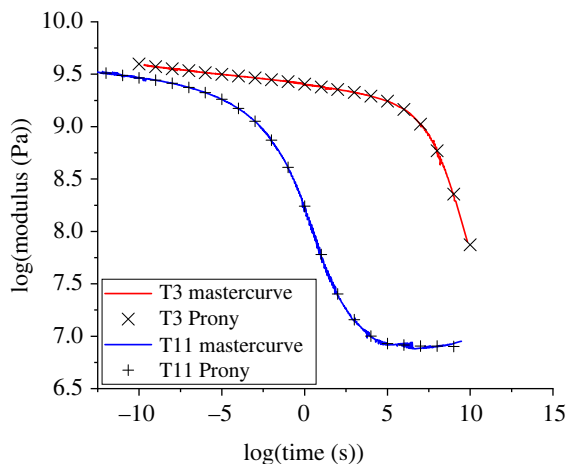


Figure 7. Mastercurves for ‘Task 11’ and ‘Task 3’ for a 20°C reference temperature from three-point bend DMA compared to the Prony fit to these curves using branches with relaxation times spaced one per decade.

in machine compliance and to the lack of clamping effecting in the three-point bend configuration compared to the single cantilever [28]. For these reasons, data from the three-point bend configuration were used to calibrate the Prony model, figure 7.

The mastercurves for both polymers are shown in figure 7 along with the Prony fits. Both polymers have similar overall behaviours, with the glass transition and no secondary transitions over the frequency range explored. At small relaxation times, i.e. below the glass transition, the stiffnesses of the polymers begin to converge, which is expected due to their chemical similarity. It is also expected that the stiffnesses would converge at long relaxation times had suitable data been obtained, however, such data is out of the scope of this project.

It is observed that Task 11 is the less stiff of the two polymers; at timescales on the order of seconds, it is within its glass transition and is highly rate sensitive. At similar timescales, Task 3 is below its glass transition and is, therefore, stiffer and less rate sensitive than Task 11.

To produce the Prony series representations equation (4.1) was fitted to the mastercurves using the curve fitting toolbox in Matlab®. The number of branches was set so that their characteristic times, as defined by equation (4.2), were spaced by one decade. Hence, a 22-branch and a 24-branch Prony series were fitted to Task 3 and Task 11, respectively; the predicted moduli at a number of frequencies are shown in figure 7, while the Prony parameters alongside further material properties are presented in the electronic supplementary material, Appendix.

(b) Large strain compression

The low- and high-strain rate compression results obtained at 20°C are shown in figure 8. Low-rate results from experiments at sub-ambient temperatures are presented in figure 9.

There were distinctly different behaviours when comparing the low-strain rate behaviour of the two polymers. The initial stiffness of Task 3, figure 8*a*, was relatively rate insensitive, consistent with the DMA results. This polymer exhibited yielding, confirmed by measurement of permanent deformation of recovered specimens. This yield stress was rate sensitive and increased from around 80 to 110 MPa over the range of strain rates tested, figure 10. For Task 11, significant rate sensitivity was observed, figure 11, again consistent with the DMA data. However, no yielding was observed: the applied strain was fully recovered.

At sub-ambient temperatures, Task 3 exhibited minor sensitivity of initial stiffness but significant variation in yield stress, which increased from 80 MPa to 200 MPa over the temperature range explored, figure 12. The post-yield behaviour also depended on temperature, with the

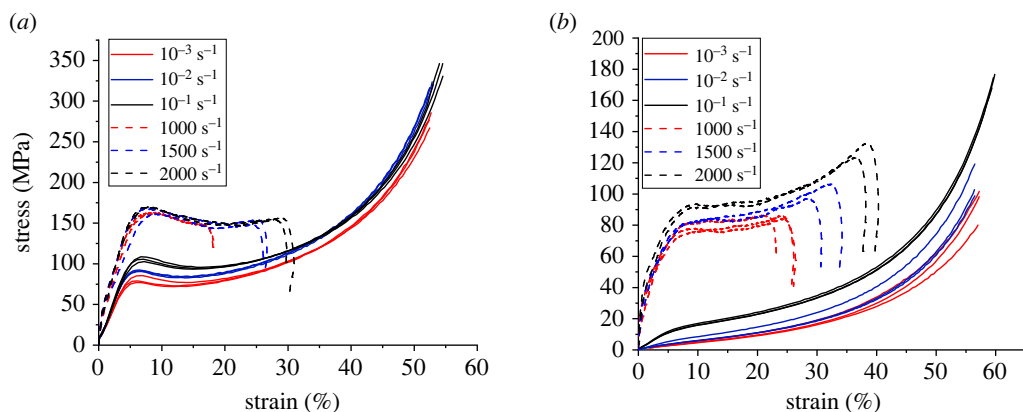


Figure 8. Stress–strain curves from low- and high-rate characterization at room temperature. In all cases, the end of the curve represents the end of loading, the specimens did not fail. (a) Task 3 and (b) Task 11.

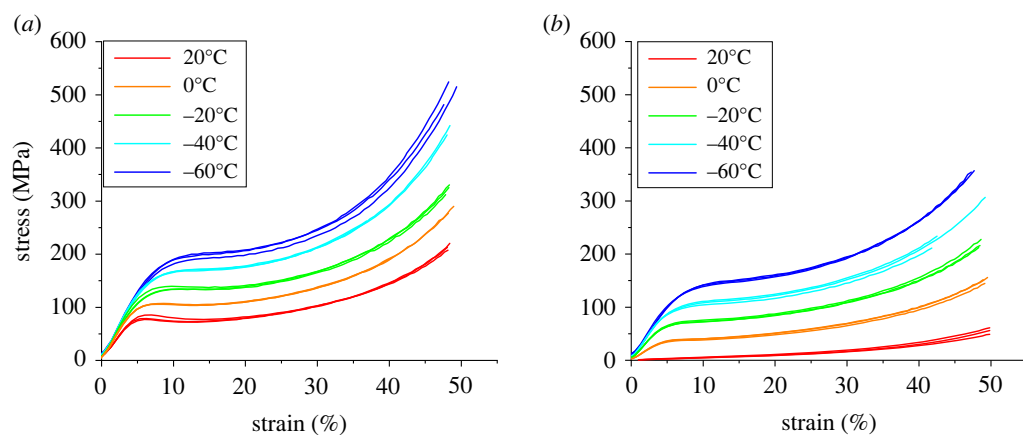


Figure 9. Stress–strain response of both polymers in compression at sub-ambient temperatures and 10^{-3} s^{-1} . (a) Task 3 and (b) Task 11.

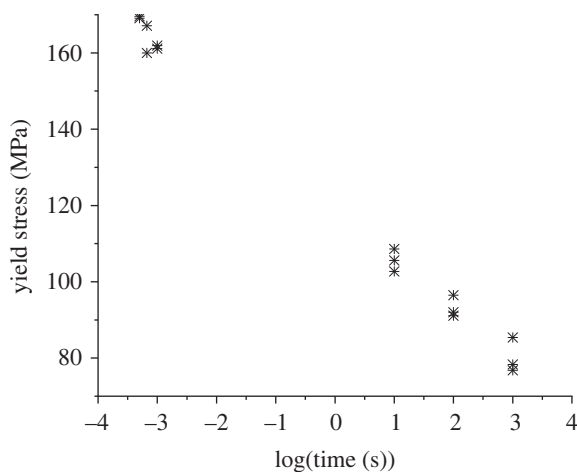


Figure 10. Yield stress of Task 3 with varying loading time.

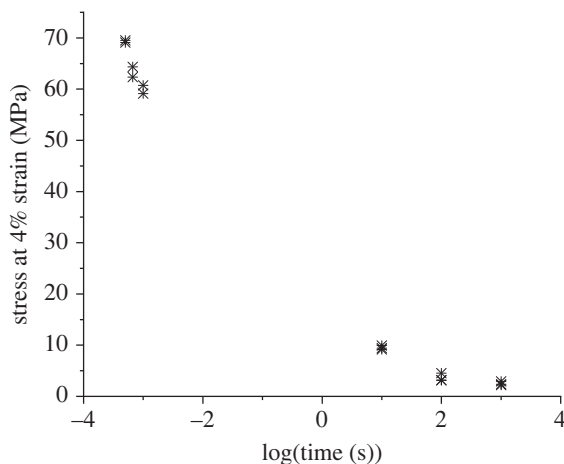


Figure 11. Variation of stress of Task 11 at 4% strain with loading time. Note this polymer does not have a yield point.

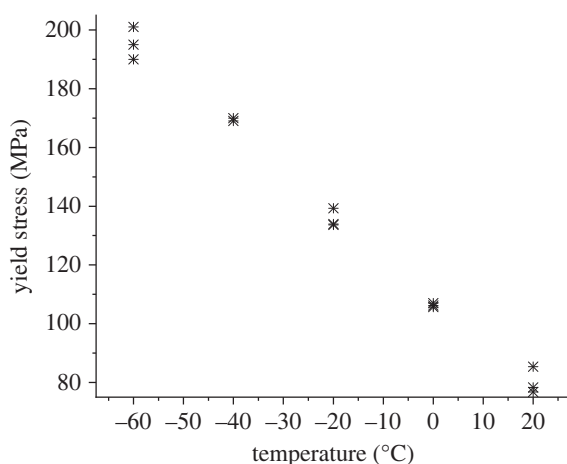


Figure 12. Yield strength of Task 3 with varying temperature.

amount of softening reducing as the temperature decreased. For Task 11, there was significant temperature sensitivity, figure 13: the stiffness increased by an order of magnitude over the temperature range explored and nonlinear, but still fully recoverable, behaviour was observed. Note that the yield stress of Task 11 at the lowest temperature is similar to Task 3 at the highest temperature; this is consistent with the DMA results that show the two polymers having similar behaviours below their glass transition.

Comparing the high-strain rate response, Task 3 exhibited increased stiffness compared to that observed in the low-rate experiment and yielded at a stress of approximately 160 MPa. Over the full range of strain rates tested, the yield stress appears to be approximately linear in $\log(\text{strain rate})$. For Task 11, there was a significant increase in stiffness compared to the low-rate experiments, as the polymer moved through the glass transition. Although the polymer displays nonlinearity above a strain of approximately 5%, the deformation remained fully recoverable, displaying behaviour akin to ‘leathery’ as described by Boyce [29].

Interestingly, the low-rate experiments on Task 3, $\log(t) \sim 2$, and the high-rate experiments on Task 11, $\log(t) \sim -6$, correspond to similar positions for each polymer on their mastercurves, figure 7. In both cases, the timescales are within the region of glassy response, and, therefore, the polymers might be expected to exhibit similar behaviour. This is shown in figure 14, where the

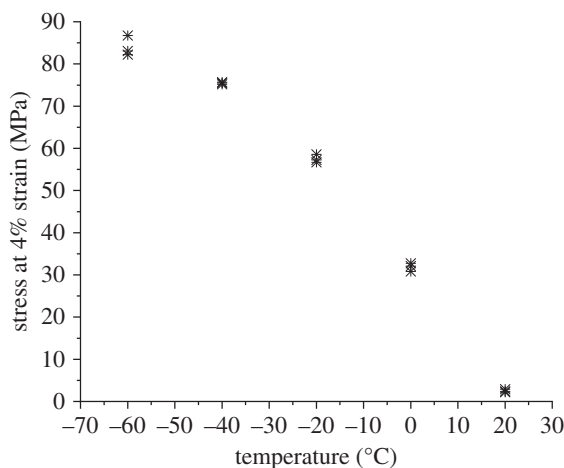


Figure 13. Variation of stress of Task 11 at 4% strain with temperature.

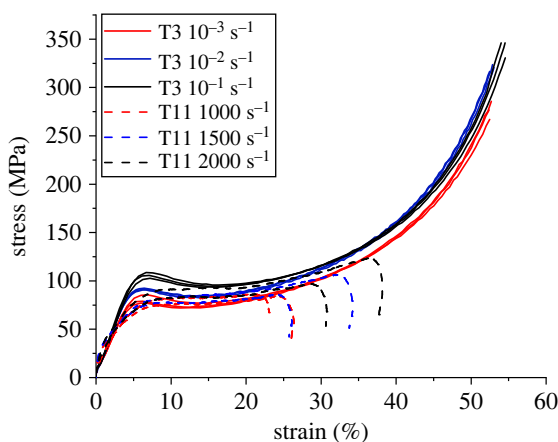


Figure 14. Comparison of stress–strain curves for Task 3 at low-strain rates and Task 11 at high rates. These two different polymers exhibit similar behaviours when the α motions (which govern the glass transition) are restricted.

stress–strain curves of the polymers are overlain. The main difference between the two is that Task 3 exhibits a peak (attributed to yielding) followed by strain softening, which is not seen in Task 11; it was also observed that Task 3 showed irrecoverable strain, while Task 11 did not. It must be noted that, in Task 11, *during the deformation*, structural relaxations associated with the glass transition cannot take place, but these relaxations can take place before and after the deformation. Hence, Task 11 starts and ends with its structure in a state of thermal equilibrium (because the room temperature is above the glass transition temperature), whereas Task 3 does not, because room temperature is below the glass transition and hence the structure is never in equilibrium.

A further comparison was performed between the low-temperature and high-strain rate behaviour of each polymer, [figure 15](#). As expected, the apparent stiffnesses and yield stresses agree at appropriate conditions. For Task 11, there is a good match for the whole of the stress–strain response, for Task 3 this is not the case, the curves obtained from the high-rate experiments soften considerably. One phenomenon of high-strain rate testing is that the temperature in the specimen increases if mechanical work is converted to heat, because the heat does not have time to leave the specimen on the timescale of the loading. This would reduce the stress supported by

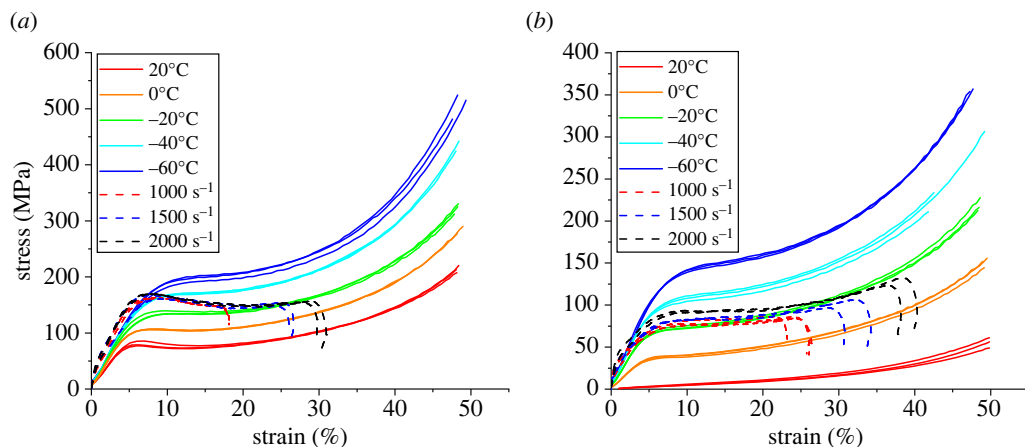


Figure 15. Comparison between high-rate experiments performed under ambient conditions and low-rate (10^{-3} s^{-1}) experiments performed at sub-ambient temperatures. (a) Task 3 and (b) Task 11.

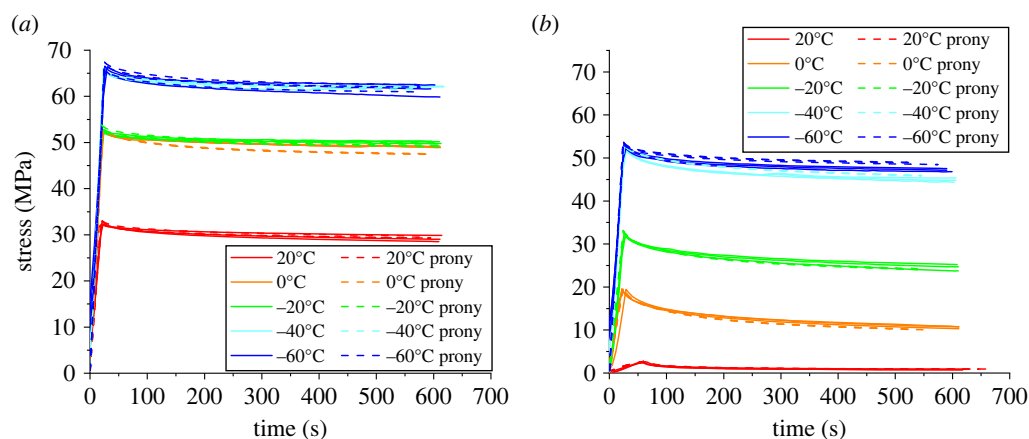


Figure 16. Stress-time relaxation response for Task 3 and 11. (a) T3 stress-time and (b) T11 stress-time.

the specimen. This may be the case in the Task 3 specimens and would be consistent with these specimens showing irrecoverable (plastic) deformation that is not observed in Task 11.

(c) Low-rate relaxation response

(i) Low-temperature small-strain relaxation

The relaxation behaviour was measured at ambient and sub-ambient conditions and compared to predictions from the Prony model. Specimens were compressed to a pre-defined load, after which the crosshead was fixed in position, and the polymer was allowed to relax for 10 min. The load was selected, based on data in figure 9, to ensure that the polymer did not yield.

The stress-time response for each polymer during loading and relaxation is presented in figure 16*a,b*. To enable comparisons, these data are normalized to the peak stress under each loading condition, figure 17; the stress-strain response is shown in figure 18. In all cases, the experimental data were compared to predictions from the Prony model.

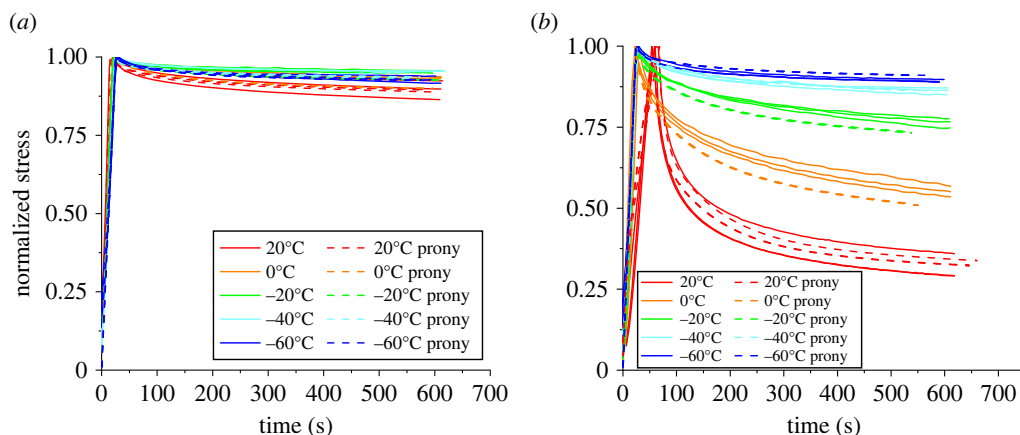


Figure 17. Stress-time relaxation response for Task 3 and 11. The response has been normalized to the peak stress observed at each condition. (a) Normalized T3 Stress-time. (b) Normalized T11 Stress-time.

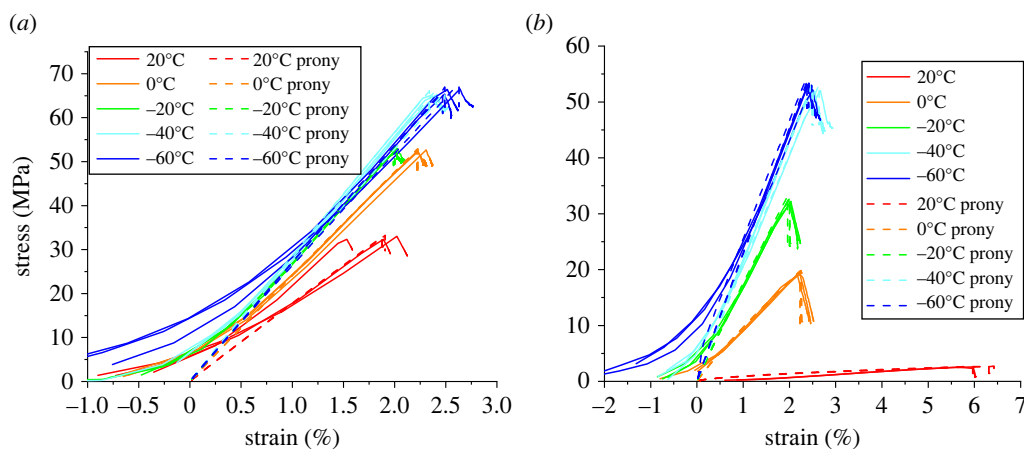


Figure 18. Stress-strain relaxation response for Task 3 and 11. (a) T3 Stress-strain and (b) T11 Stress-strain.

For each of these experiments, the variation in modulus over time (defined as the stress divided by the strain) was calculated and compared to the mastercurves of each polymer, figure 19. For each temperature, the previously calculated shift factors, derived using DMA and displayed in figure 5, have been applied.

For the stress-time behaviour of Task 3, figure 16a and figure 15a, little relaxation was observed at all temperatures, and this appeared to be relatively temperature independent. The polymer was above its glass transition at these temperatures, as shown in figure 19a, so these results were expected. Conversely, Task 11 displayed a broad range of relaxation behaviour, figure 16b and figure 15b. This polymer moved through its glass transition, figure 19b, so the behaviour is highly temperature dependent.

The model accurately predicts the stress-relaxation of both polymers under these conditions. There is a remarkably good fit for Task 11, particularly because this range of conditions captures the polymer's behaviour through the glass transition region and the relatively large relaxations. This is encouraging because the behaviour in this transition region is highly sensitive to the environmental conditions. The strain-strain behaviour, figure 18, shows that the model gives a lower strain upon loading; however, because the model follows the experimental stress relaxation

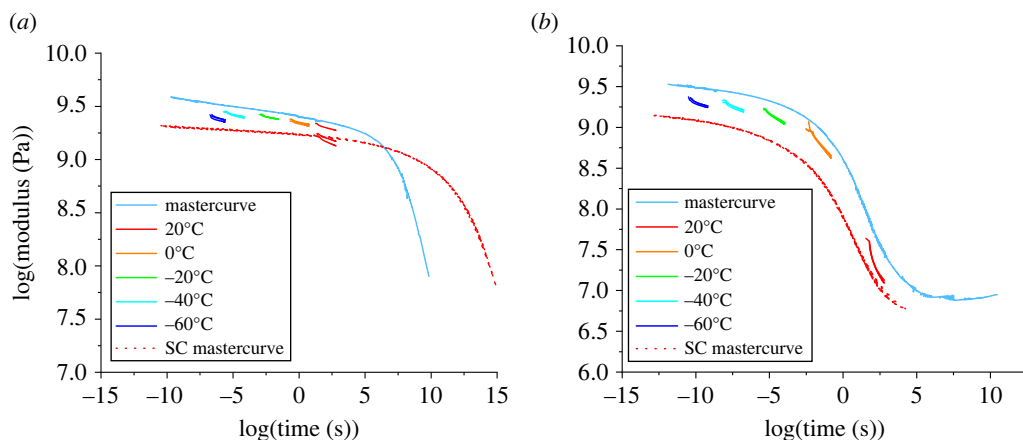


Figure 19. Low-temperature relaxation data overlain on the polymer mastercurves generated from DMA experiments in three-point bend and single cantilever. The low-temperature curves have been shifted by their corresponding shift factors. (a) Task 3 and (b) Task 11.

profile, this difference is simply a proportional factor in the modulus. It is well established that strains are difficult to measure in compression experiments [30], and that the measured values are typically too high because of end effects introduced by the lubricant layer and machining tolerances; one effect of this is the ‘toeing in’ at the start of each of the experimental curves. This justifies the use of force, rather than strain, targets in both the experiments and modelling. The difference in modulus is clear in figure 19. Further, figure 19 confirms the observation from [28] that the three-point bend mastercurve (obtained using relaxation measurements) matched experimental data better than did the mastercurve from the single-cantilever experiments (in which oscillatory loading was used). Finally, taken as a whole, these data support this strategy for predicting relaxations from DMA experiments.

Finally, it can be observed that, during relaxation, the assumption that the boundaries remain fixed is not strictly true. Inspection of the stress–strain curves, for which strains are measured using contacting extensometers attached to the loading anvils close to the specimen, reveal that the strain increased slightly. This was due to the compliance of the load chain, which expanded into the specimen as the load reduces, even if the crosshead was fixed. This effect will cause a slight increase in the observed stress during relaxation, which may further explain some of the discrepancies between the model and experimental results.

These results show that the Prony model can accurately capture the polymer stress relaxation behaviour under loading and relaxation. This is encouraging; however, only small-strain behaviour has been examined. Therefore, an investigation was performed at higher strains, chosen to match the final strains in the high-rate relaxation experiments in §3b(ii).

(ii) Room temperature large strain response

Specimens were deformed to strains of 4% and 10% (Task 3) and 10% and 15% (Task 11) at ambient temperature. These strains were chosen to match those obtained in the interrupted Hopkinson bar experiments, described later, to allow comparison between low-rate and dynamic loading. In order to simulate these experiments, the boundary conditions for the model were modified to accommodate the nonlinear (e.g. plastic) behaviour without having to produce a full viscoelastic-viscoplastic model. The model was again ‘loaded’ to the same stress as the experiment, before being allowed to relax with fixed boundaries. Effectively, the assumption was made that the total

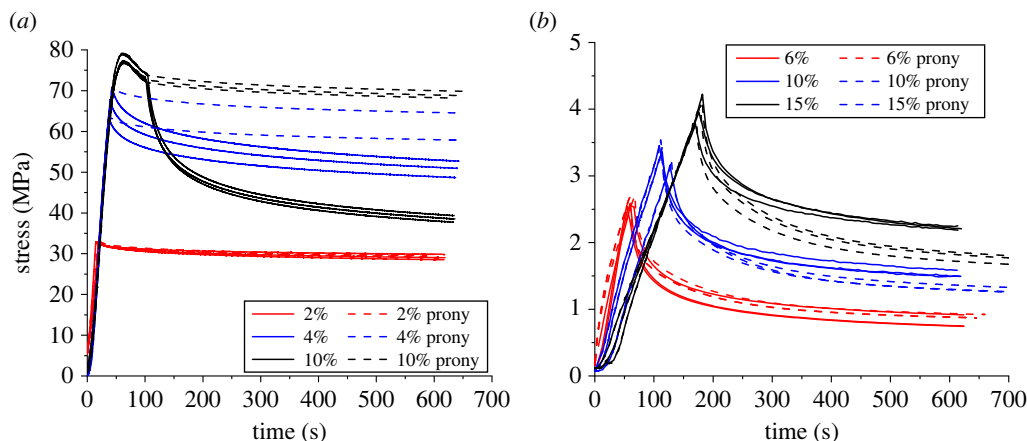


Figure 20. Stress-time behaviour for Task 3 and Task 11. Specimens were now loaded to larger strains before relaxation. (a) T3 Stress-time, (b) T11 Stress-time.

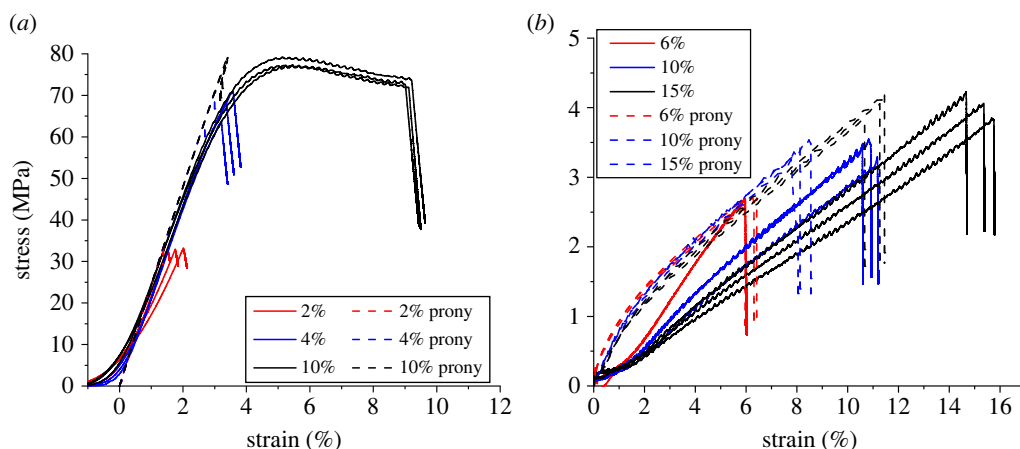


Figure 21. Stress-strain response for Task 3 and Task 11. (a) T3 Stress-strain, (b) T11 Stress-strain. (Online version in colour.)

strain comprised the sum of plastic and elastic strains, and it was the relaxation of the elastic component that governed the overall relaxation behaviour.

The stress-time behaviour of Task 3 loaded to three stresses before being allowed to relax is shown in figure 20*a*. The relaxation behaviour of the polymer is dependent upon the applied strain, with greater relaxation as the strain increases. Here, the Prony model can no longer accurately predict the relaxation, indicating that the assumptions above are not appropriate and that the onset of plasticity needs to be considered. The data for Task 11, figure 20*b*, support this observation. Here, the Prony model can still accurately predict the polymer's relaxation response at strains two orders of magnitude greater than those used in the characterization experiments from which it was derived.

The stress-strain behaviours of Task 3 and Task 11 are shown in figure 21*a,b*, respectively. Due to the plasticity in Task 3, the model comparison to the experimental stress-strain response is highly inaccurate, whereas, for Task 11, the model can still predict the stress-strain response reasonably reliably.

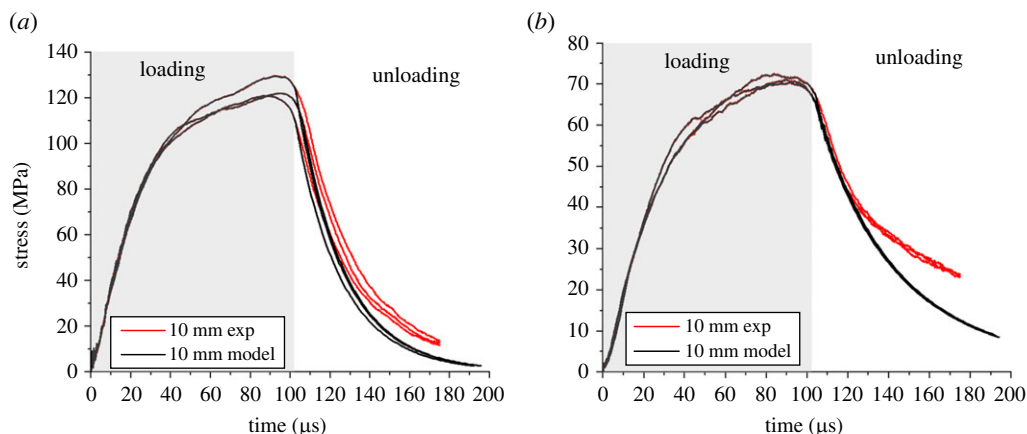


Figure 22. Stress-time dynamic relaxation response of 10 mm diameter specimens. The model was loaded using the stress-time profile from the experiment. Relaxation was allowed to occur under the confining force of two dashpots. (a) Task 3 and (b) Task 11.

(c) High-rate relaxation response

A Hopkinson bar was used to explore the relaxation of the polymer on microsecond timescales and to investigate the Prony model's ability to predict the behaviour. The same apparatus was used as the previous Hopkinson bar experiments; however, now a 250 mm striker bar was employed. This allowed a gap between wave oscillations in the system, giving a greater period of time to capture the dynamic relaxation response of the polymer. Two specimen geometries were used, both 3.5 mm long: 10 mm and 6 mm in diameter. The two sizes allowed an investigation into the effect of final strain to be conducted.

To model this experiment, the Prony series was loaded using the stress boundary conditions measured in the experiment and then allowed to expand as if they were restricted by two dashpots, as described in §4.3. For comparison, model results were also obtained using fixed and free boundary conditions.

(i) Ten millimeter specimens

The 10 mm diameter specimen results are shown as stress-time, strain-time and stress-strain plots, and compared to the model predictions, in figures 22–24. For both polymers, the Prony series representation was loaded using the measured stress-time boundary conditions. Once the peak stress was achieved, the model could relax under the confining force of two dashpots [25].

There are interesting comparisons that can be made between these materials. For Task 3, the model was able to predict accurately the measured relaxation behaviour. The model overpredicted the loading modulus slightly; this is consistent with the result previously observed in the sub-ambient relaxation experiments, figure 19a. The effect of heating within the polymer during loading was also checked. Using a heat capacity of $1.38 \text{ J g}^{-1} \text{ K}^{-1}$, taken from DSC experiments, the maximum temperature rise, if all applied work was converted to heat, was 2°C . This heating was simulated; however, it was found to have a negligible effect on the response.

The model also captured the stress-time relaxation response of Task 11, but significantly underpredicted the strain. This observation of a modulus significantly greater than predicted agrees with the previously observed room temperature relaxation behaviour, figure 19b. The model's ability to predict the stress-time response is encouraging because this suggests the Prony model can predict the stress relaxation response of the material well; however, there is a proportional offset in the stiffness which should be accounted for. Interestingly, from figure 22b,

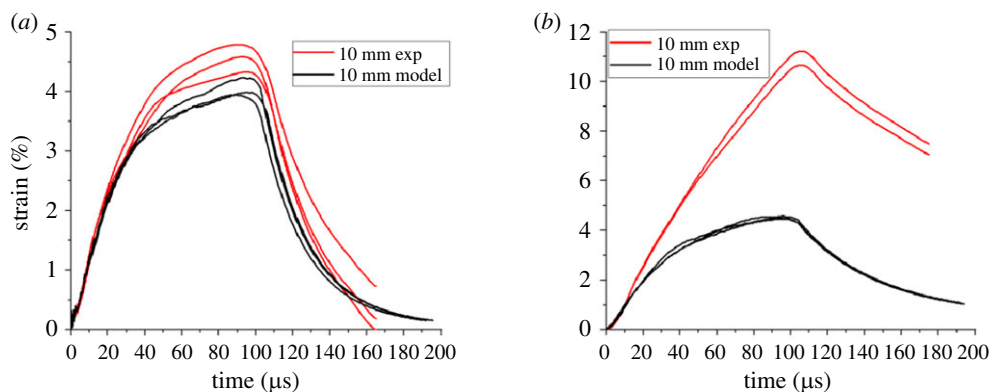


Figure 23. Strain-time dynamic relaxation response of 10 mm diameter specimens. (a) Task 3 and (b) Task 11.

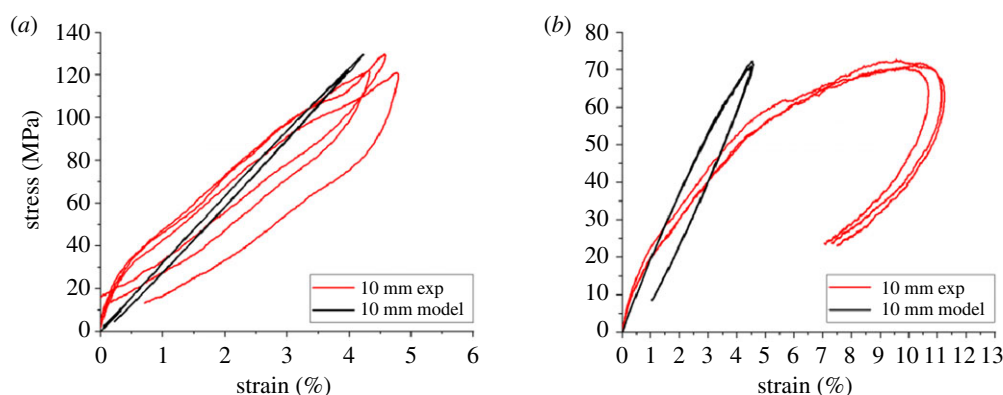


Figure 24. Stress-strain response of 10 mm diameter specimens. (a) Task 3 and (b) Task 11.

there appears to be an emergence of a two-phase relaxation. The model can accurately predict the first phase of relaxation well but as the polymer relaxes further, there appears to be a step change in gradient and the polymer deviates from the model. This is in contrast with the behaviour presented in Task 3, figure 22a, in which no step change is observed and the model can accurately predict the polymer's stress behaviour under near full relaxation.

A further investigation was conducted into the influence of the model's boundary conditions upon relaxation. The dashpot boundary conditions were applied to the model, calculated using the mechanical and geometric properties of the bar and specimens, as well as fixed and free boundary conditions. The results are presented in figure 25. Under fixed boundary conditions, the model significantly overpredicts the stress. Interestingly, these boundaries cause a relaxation tangential to the stress-time curve at peak stress. This showed that as the confining bars change from loading to unloading the specimen, there is a finite period of time in which they do act as approximately immovable, and the polymer relaxes under fixed conditions. Under free boundary conditions, the model relaxes nearly instantaneously, which because of the mass of the specimens causes the stress to oscillate around zero. A further investigation was conducted into the model's sensitivity to the value of the constraining dashpots' viscosity by varying this value by $\pm 10\%$. It was found that the variation of relaxation response (highlighted in blue) was relatively insensitive to variations in this value.

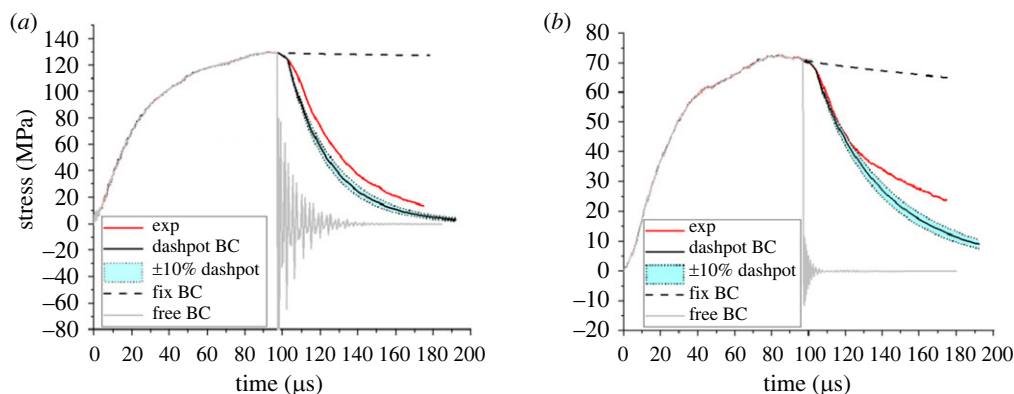


Figure 25. Modelled stress-time response during relaxation with various boundary conditions applied. (a) Task 3 and (b) Task 11.

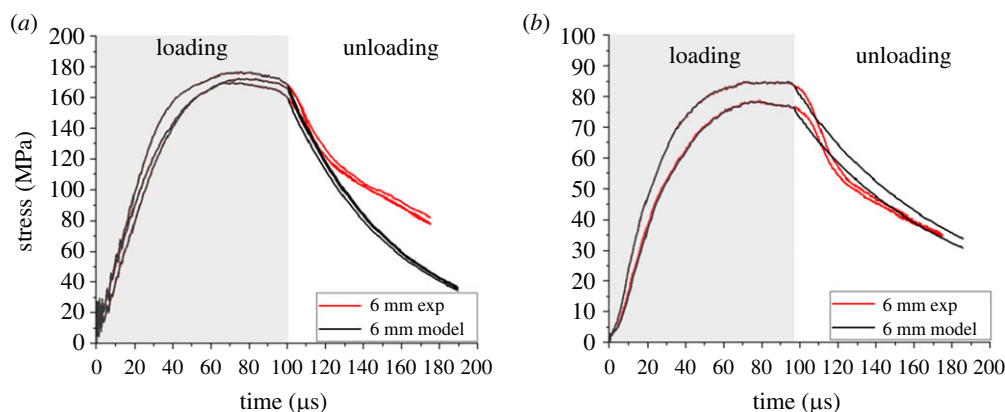


Figure 26. Stress-time dynamic relaxation response of 6 mm diameter specimens. (a) Task 3 and (b) Task 11.

(ii) Six millimeter specimens

The Hopkinson bar experiments were repeated using 6 mm diameter specimens, allowing the influence of larger strains to be investigated. The results are presented in figures 26–28.

For Task 3, plasticity is now exhibited. The model can still predict the relaxation stress-time behaviour, figure 26*a*, during the early phase of relaxation, but as the time increases, the polymer relaxed less than predicted. For Task 11, the model works well overall but appears to miss a high-frequency component of the experimental relaxation. The strain was far greater than was expected as the experimental Task 11 had a greater modulus than expected, as observed before.

Figure 29 displays overlain relaxation responses following high-strain rate loading for both specimen geometries used. For comparison, the stress has been normalized to the value at the onset of relaxation. For both polymers, the relaxation for the 6 mm specimens, which were loaded to larger strains, is slower than for the 10 mm; the models capture this behaviour. Experimentally, the smaller area specimens exert less force on the confining bars, reducing their expansion and causing the specimen to relax more slowly. The model reflects this in the calculation of the viscosity of the confining dashpots.

As the relaxation progresses, there is evidence of a two-phase relaxation. In general, the model captured the initial phase of the relaxation well, indicating linear-viscoelastic behaviour here. As the relaxation progressed, there was a rapid change in the experimental gradient, causing

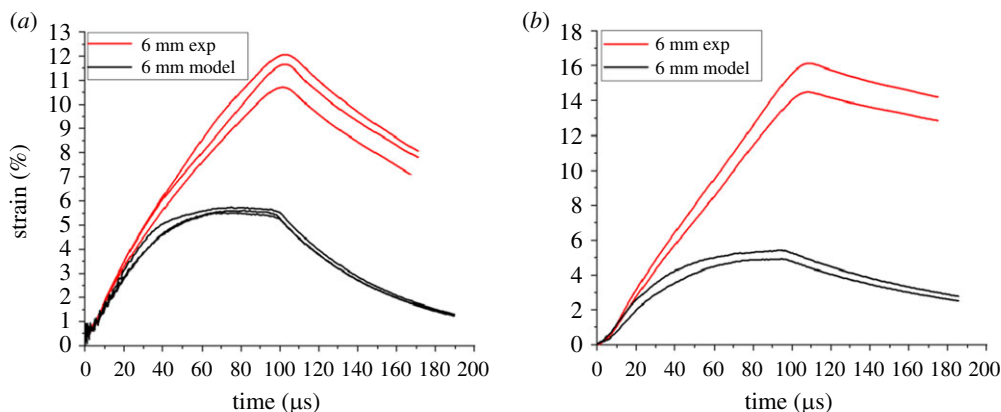


Figure 27. Strain-time dynamic relaxation response of 6 mm diameter specimens. (a) Task 3 and (b) Task 11.

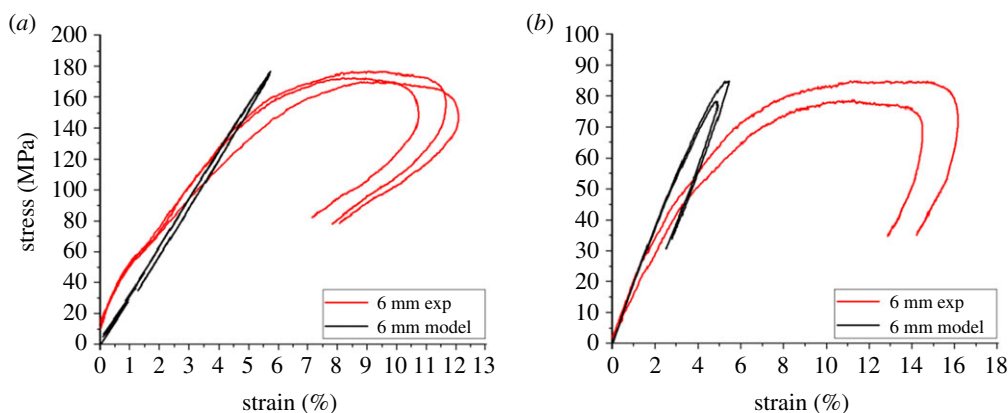


Figure 28. Stress-strain response of Task 3 and Task 11 at high rate with 6 mm geometry. (a) Task 3 and (b) Task 11.

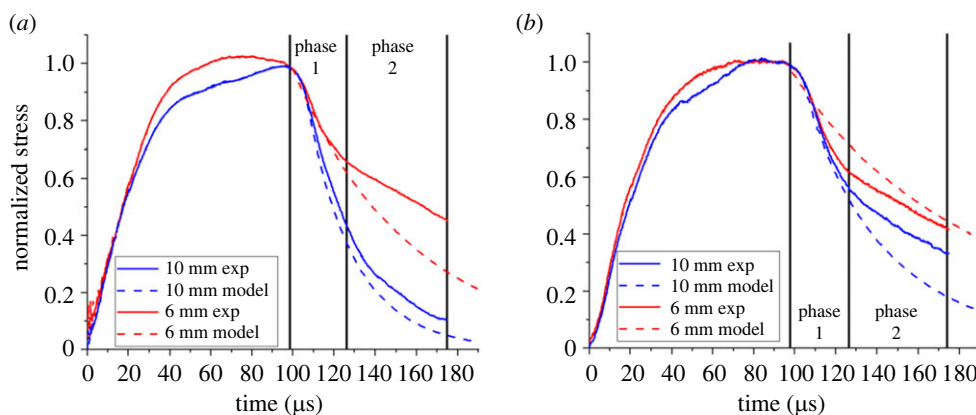


Figure 29. Stress-time response comparing individual 10 mm and 6 mm high-rate relaxation specimens for Task 3 and Task 11. The stress has been normalized to the stress at the onset of relaxation. (a) Task 3 and (b) Task 11.

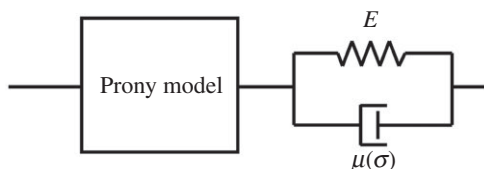


Figure 30. Modified polymer model to account for low- and high-rate nonlinearities.

a divergence between experiment and model. Broadly, this two-phase response became more pronounced at greater strains. The change in relaxation response could be due to a boundary condition change or a deviation from linear viscoelasticity. The boundary conditions would have evolved during the experiment as the dimensions of the specimen changed. However, this would have been unlikely to produce a significant gradient step change, as was observed here. Therefore, it is believed that a deviation from linear viscoelasticity took place at large strains.

For Task 3, these nonlinear effects appear to become activated alongside plasticity because this phenomenon was not observed in the 10 mm specimen, which did not yield, but was present in the 6 mm. For Task 11, the effects are present in both specimens. Interestingly, the initial relaxation of this polymer is nearly independent of specimen diameter. Further, no yielding was observed in Task 11, therefore, it is thought that any nonlinear processes which caused this effect were a function of increasing strain and included but were not limited to plasticity.

6. Discussion

The data above allow a range of comparisons to be made: between different materials; between different timescales; and between model and experiment. Broadly, the model was able to predict the relaxation behaviour of both polymers at low and high rates; however, when the polymer exhibited plasticity, the experiment and the model deviated. This study focused on a broad range of experimental conditions and, hence, only 2–3 specimens were investigated under each loading or environmental condition. Despite the relatively low number of specimens, the results were found to be generally repeatable where at worst, observed during the dynamic relaxation experiment, inter-specimen variation was around 10–15%. However, many conditions exhibited smaller inter-specimen variation than this.

Considering the relaxation of Task 3 following loading to larger strains, generally the model overpredicts the amount of relaxation in the high-rate experiments, and under-predicts at low rate, *figure 20*. In particular, in the low rate as the strain increased and became closer to the yield point, the amount of stress relaxation increased significantly and was far more than predicted. For Task 11, even at these increased strains, the ability of the model to capture the stress relaxation response was very good.

From these observations, modifications to the model are proposed, *figure 30*, but were not implemented. These would take the form of a spring and dashpot pairing in series to the original Prony model and the pairing would have a characteristic time constant between 100 μ s and 100 s. The viscosity of the dashpot would be stress dependent and would reduce at large stresses. At low rate, when the material model is relaxing under the restriction of fixed boundary conditions, this would allow the model to relax faster than the Prony series alone. At high rates, when the model is relaxing under the limitation of two external dashpots, this would act to reduce the stiffness of the combined model and thus slow the expansion. However, the exact formulation of this model is beyond the scope of this research.

7. Conclusion

In this study, the stress relaxation behaviour of two selected PUs was investigated following loading at low and high rates and modelled using a Prony series model calibrated using data from

DMA experiments. Two geometries of DMA were used: single-cantilever and three-point bend, the latter found to produce modulus values closer to those determined in other experiments.

Monotonic compression and stress relaxation experiments were conducted at low rate over a range of temperatures. It was found that the Prony model accurately predicted the stress relaxation behaviour, even through the glass transition. Further low-rate experiments were conducted at larger strains and the model was found to predict relaxation well provided the polymer did not yield. Once yielding occurred, the polymer relaxed more rapidly than predicted.

The monotonic compression experiments at different temperatures and strain rates showed well the equivalence of low-temperature low-rate experiments and ambient temperature dynamic experiments. They also showed the equivalence between the two polymers of similar structure but different glass transition temperatures, at appropriate combinations of temperature and rate.

Dynamic relaxation experiments were conducted on a Hopkinson bar. The model was able to capture the relaxation response of the PUs during the early phase of relaxation. The boundaries introduced by the Hopkinson bars during relaxation were successfully modelled using dashpots of appropriate viscosity; however, a sharp change in gradient observed during the relaxation was not predicted by the model. This change in gradient was exacerbated with increasing loading strain. It was suggested during early stages of relaxation that the material obeyed linear viscoelasticity with which the model was derived. However, various nonlinear viscous processes in the material became activated during loading and became increasingly influential at larger strains. It may be possible to capture this behaviour in a nonlinear viscoelastic model by means of the addition of a parallel spring-dashpot pairing whose viscosity is stress dependent. However, the exact modifications are outside the scope of this research.

In addition to providing data on the response of these polymers, this paper demonstrates that relaxation after dynamic loading has the potential to provide a direct alternative to indirect measurements of short timescale polymer response using time-temperature superposition.

Data accessibility. The datasets supporting this article have been uploaded as part of the electronic supplementary material [31].

Authors' contributions. T.C.: conceptualization, data curation, formal analysis, investigation, methodology, validation, writing—original draft and writing—review and editing; C.R.S.: conceptualization, funding acquisition, methodology, project administration, resources, supervision, validation, visualization and writing—review and editing.

Both authors gave final approval for publication and agreed to be held accountable for the work performed therein.

Conflict of interest declaration. We declare we have no competing interests.

Funding. The authors would like to thank Dstl, in particular Rebecca Livesey and Neil Middleton, for their financial and intellectual support during this work under contract no. DSTLX1000128371.

Acknowledgements. Additionally, thanks must be extended to Igor Dyson and Nick Hawkins for their experimental and analytical assistance as well as Neil Warland and Andy Bateman for specimen manufacture. For the purpose of Open Access, the author has applied a CC BY public copyright license to any Author Accepted Manuscript (AAM) version arising from this submission.

References

1. Nurazzi NM *et al.* 2021 A review on natural fiber reinforced polymer composite for bullet proof and ballistic applications. *Polymers (Basel)* **13**, 1–42. (doi:10.3390/polym13040646)
2. Aisyah HA, Paridah MT, Sapuan SM, Ilyas RA, Khalina A, Nurazzi NM, Lee SH, Lee CH. 2021 A comprehensive review on advanced sustainable woven natural fibre polymer composites. *Polymers* **13**, 1–45. (doi:10.3390/polym13030471)
3. García JM, García FC, Serna F, de la Peña JL. 2010 High-performance aromatic polyamides. *Prog. Polym. Sci. (Oxford)* **35**, 623–686. (doi:10.1016/j.progpolymsci.2009.09.002)
4. Groh KJ *et al.* 2019 Overview of known plastic packaging-associated chemicals and their hazards. *Sci. Total Environ.* **651**, 3253–3268. (doi:10.1016/j.scitotenv.2018.10.015)
5. Bugnicourt E, Cinelli P, Lazzeri A, Alvarez V. 2014 Polyhydroxyalkanoate (PHA): review of synthesis, characteristics, processing and potential applications in packaging. *Express Polym. Lett.* **8**, 791–808. (doi:10.3144/expresspolymlett.2014.82)

6. Akella K, Naik NK. 2015 Composite armour—A review. *J. Indian Inst. Sci.* **95**, 297–312.
7. Okereke MI, Buckley CP, Siviour CR. 2012 Compression of polypropylene across a wide range of strain rates. *Mech. Time Depend. Mater.* **16**, 361–379. (doi:10.1007/s11043-012-9167-z)
8. Tschoegl NW, Knauss WG, Emri I. 2002 The effect of temperature and pressure on the mechanical properties of thermo- and/or piezorheologically simple polymeric materials in thermodynamic equilibrium - a critical review. *Mech. Time Depend. Mater.* **6**, 53–99. (doi:10.1023/A:1014421519100)
9. Doi M, Takimoto JI. 2003 Molecular modelling of entanglement. *Phil. Trans. R. Soc. A* **361**, 641–652. (doi:10.1098/rsta.2002.1168)
10. Ortiz C, Kim R, Rodighiero E, Ober CK, Kramer EJ. 1998 Deformation of a Polydomain, Liquid Crystalline Epoxy-Based Thermoset. *Macromolecules* **31**, 4074–4088.
11. David NV, Gao XL, Zheng JQ. 2011 Stress relaxation of a Twaron® /natural rubber composite. *J. Eng. Mater. Technol.* **133**, 011001. (doi:10.1115/1.4002636)
12. Björk F, Stenberg B. 1990 Stress relaxation of a nitrile rubber surrounded by an oil that increases the network density. *Polymer (Guildf)* **31**, 1649–1657.
13. Sperling LH. 2005 *Introduction to physical polymer science*. New York, NY: John Wiley & Sons.
14. Arzhakov M. 2019 *Relaxation in physical and mechanical behavior of polymers*. Boca Raton, FL: CRC Press.
15. Wineman AS, Rajagopal KR. 2000 *Mechanical response of polymers*. Cambridge, UK: Cambridge University Press.
16. Taylor RL, Pister KS, Goudreau GL. 1970 Thermomechanical analysis of viscoelastic solids. *Int. J. Numer. Methods Eng.* **2**, 45–59.
17. Park SW, Schapery RA. 1999 Methods of interconversion between linear viscoelastic material functions. Part I—a numerical method based on Prony series. *Int. J. Solids Struct.* **36**, 1653–1675. (doi:10.1016/S0020-7683(98)00055-9)
18. Saba N, Jawaidd M, Alothman OY, Paridah MT. 2016 A review on dynamic mechanical properties of natural fibre reinforced polymer composites. *Construct. Build. Mater.* **106**, 149–159. (doi:10.1016/j.conbuildmat.2015.12.075)
19. Williams ML, Landel RF, Ferry JD. 1955 The temperature dependence of relaxation mechanisms in amorphous polymers and other glass-forming liquids. *J. Am. Chem. Soc.* **77**, 3701–3707.
20. Kolsky H. 1949 An investigation of the mechanical properties of materials at very high rates of loading. *Proc. Phys. Soc. Sect. B* **62**, 676–700. (doi:10.1088/0370-1301/62/11/302)
21. Gray G, Blumenthal WR. 2000 Split-Hopkinson pressure bar testing of soft materials. *Mech. Test. Evaluat.* **8**, 1093–1114.
22. Field JE, Walley SM, Proud WG, Goldrein HT, Siviour CR. 2004 Review of experimental techniques for high rate deformation and shock studies. *Int. J. Impact Eng.* **30**, 725–775. (doi:10.1016/j.jimpeng.2004.03.005)
23. Chen WW, Song B. 2010 *Split Hopkinson (Kolsky) bar: design, testing and applications*. New York, NY: Springer Science & Business Media.
24. Song B, Chen W. 2005 Split Hopkinson pressure bar techniques for characterizing soft materials. *Latin Am. J. Solids Struct.* **2**, 113–152.
25. Loete TJC, Paul G, Ismail EB. 2015 A preliminary investigation of the dynamic viscoelastic relaxation of bovine cortical bone. *EPJ Web Conf. EDP Sci.* **94**, 03004. (doi:10.1051/epjconf/20159403004)
26. Bentley Advanced Materials. See <https://www.benam.co.uk/products/plastic/task>.
27. McCrum NG, Buckley CP, Bucknall CB. 1997 *Principles of polymer engineering*. Oxford, UK: Oxford University Press.
28. Deng S, Hou M, Ye L. 2007 Temperature-dependent elastic moduli of epoxies measured by DMA and their correlations to mechanical testing data. *Polym. Test.* **26**, 803–813. (doi:10.1016/j.polymertesting.2007.05.003)
29. Yi J, Boyce MC, Lee GF, Balizer E. 2006 Large deformation rate-dependent stress-strain behavior of polyurea and polyurethanes. *Polymer (Guildf)* **47**, 319–329. (doi:10.1016/j.polymer.2005.10.107)
30. Li P, Siviour CR, Petrinic N. 2009 The effect of strain rate, specimen geometry and lubrication on responses of aluminium AA2024 in uniaxial compression experiments. *Exp. Mech.* **49**, 587–593. (doi:10.1007/s11340-008-9129-1)
31. Commins T, Siviour CR. 2023 Stress relaxation after low- and high-rate deformation of polyurethanes. Figshare. (doi:10.6084/m9.figshare.c.6729720)